

ShotQC: Reducing Sampling Overhead in Quantum Circuit Cutting

Po-Hung Chen
 Department of Electrical Engineering
 National Taiwan University
 Taipei, Taiwan
 b10901076@ntu.edu.tw

Dah-Wei Chiou
 Graduate Institute of Electronics
 Engineering
 National Taiwan University
 Taipei, Taiwan
 dwchiou@gmail.com

Jie-Hong Roland Jiang
 Graduate Institute of Electronics
 Engineering, Department of Electrical
 Engineering
 National Taiwan University
 Taipei, Taiwan
 jhjiang@ntu.edu.tw

Abstract

The recent *quantum circuit cutting* technique enables simulating large quantum circuits on distributed smaller devices, significantly extending the capabilities of current noisy intermediate-scale quantum (NISQ) hardware. However, this method incurs substantial classical postprocessing and additional quantum resource demands, as both postprocessing complexity and sampling overhead scale exponentially with the number of cuts introduced. In this work, we propose an enhanced circuit cutting framework *ShotQC* with effective sampling overhead reduction. It effectively reduces sampling overhead through two key optimizations: *shot distribution* and *cut parameterization*. The former employs an adaptive Monte Carlo method to dynamically allocate more quantum resources to subcircuit configurations that contribute more to variance in the final outcome. The latter leverages additional degrees of freedom in postprocessing to further suppress variance. By integrating these optimization methods, ShotQC achieves significant reductions in sampling overhead without increasing classical postprocessing complexity, as demonstrated on a range of benchmark circuits.

1 Introduction

While many promising quantum algorithms have been developed [10, 18], current quantum computers still lack the scalability and reliability needed to address practically relevant problems. Presently, most quantum devices are classified as noisy intermediate-scale quantum (NISQ) systems [17], characterized by a moderate number of qubits and limited fidelity due to noise. These devices represent an intermediate stage between classical computers and fully error-corrected quantum systems. However, their scalability is inherently constrained by the limited number of qubits and the impact of noise.

To mitigate these limitations, noise-tolerant algorithms such as the Quantum Approximate Optimization Algorithm (QAOA) [9] and the Variational Quantum Eigensolver (VQE) [16] have been developed to solve practical optimization problems on today's noisy quantum hardware. Despite these advances, scalability challenges remain a significant obstacle, restricting the advantages of quantum algorithms over

classical approaches, particularly for solving larger-scale, real-world problems.

To address these obstacles, various hybrid approaches that utilize both classical and quantum resources have been proposed. Among these, the technique of *quantum circuit cutting* has emerged as a powerful tool for enabling the simulation of large quantum circuits on smaller devices by partitioning the circuit into disconnected subcircuits, which can be executed separately and then recombined through post-processing [14]. This method not only facilitates the distribution of computational workloads across multiple smaller devices but also offers distinct advantages over executing a single large circuit. Specifically, it enhances fidelity [15, 21] and reduces noise [2], as smaller devices are typically less prone to noise. These benefits make circuit cutting a promising approach for addressing scalability challenges, particularly in the NISQ era.

The cost of circuit cutting, however, can be substantial. Specifically, the quantum resources required for repeated sampling¹ and the classical resources needed for postprocessing computations both scale exponentially with the number of cuts [5]. Consequently, identifying optimal cut points to minimize the total number of cuts is crucial [4, 19]. Other techniques, such as optimized channel decomposition [11], randomized measurements [13] and sampling-based reconstruction [12], have been proposed to mitigate the associated overhead. Furthermore, the overhead can be reduced by decreasing the size of the observable set required for each cut. State-of-the-art methods achieve this through approaches like rotating the quantum state [20], designing circuits with cutting efficiency in mind [6], or detecting optimal cut points dynamically during execution [7]. Reducing the observable set not only lowers the classical postprocessing cost but also decreases the quantum sampling overhead.

In this work, we propose an enhanced circuit cutting framework, *ShotQC*, which reduces sampling overhead by incorporating two novel techniques: *shot distribution optimization* and *cut parameterization optimization*. Shot distribution optimization is essentially an adaptive Monte Carlo

¹To accurately estimate the probability distribution of the outcomes, the circuit must be run numerous times, commonly referred to as "shots."

method that dynamically allocates different shot numbers to subcircuits, enabling more efficient variance reduction in the final outcome. Cut parameterization optimization, on the other hand, leverages additional degrees of freedom in the parameters of the mathematical identity used during postprocessing to further minimize variance.

By integrating these optimization techniques, ShotQC achieves significant reductions by up to 19x in sampling overhead without increasing the complexity of classical postprocessing, as demonstrated on a variety of benchmark circuits. Furthermore, ShotQC has multiple options that allow trade-off decisions between runtime and overhead reduction, with the economical settings still achieving a 2.6x reduction on average.

2 Quantum circuits as tensor networks

In this section, we give a brief introduction to quantum circuits in view of tensor networks. We adopt the notation used in [14], where a detailed treatment of quantum circuits as tensor networks can be found.

Any quantum circuit can be represented as a directed graph $G = (V, E)$, where the directed edges indicate the flow of qubits, and the vertices are categorized into three types: input states (denoted by \triangleleft), quantum gates (denoted by \square), and observables (denoted by \triangleright). This graph can then be converted into a tensor network $\mathcal{A} = \{A(v) : v \in V\}$, where each vertex v is associated with a tensor $A(v)$.

The set of k incoming or outgoing edges attached to a tensor is indexed by $\alpha = (\alpha_1, \alpha_2, \dots, \alpha_k)$, where each $\alpha_j \equiv (\alpha_j^1, \alpha_j^2) \in \{0, 1\}^2$ is a pair of binary indices. Let $M(\alpha) = |\alpha_1^1, \dots, \alpha_k^1\rangle\langle\alpha_1^2, \dots, \alpha_k^2|$ be the elementary matrix corresponding to α . The tensor entries of the input state ρ , the quantum gate U , and the observable O are given by

$$A(\rho)_\alpha = \text{Tr}[\rho M(\alpha)^\dagger], \quad (1a)$$

$${}_\alpha A(U)_\beta = \text{Tr}[U M(\alpha) U^\dagger M(\beta)^\dagger], \quad (1b)$$

$${}_\beta A(O) = \text{Tr}[M(\beta) O], \quad (1c)$$

where the left index of a tensor represents the incoming edges and the right index represents the outgoing edges. Using these transformations, we can evaluate the quantum circuit through its equivalent tensor network.

3 Circuit Cutting

This section presents the essential theory and an overview of circuit cutting, which decomposes identity channels into multiple *measure-and-prepare* channels.

3.1 Theory

In circuit cutting, the primary goal is to reconstruct the probability distribution of the original (uncut) circuit from those of the subcircuits. This can be achieved by computing the value of the tensor network via the lemma presented below.

For any arbitrary 2×2 matrix A , if it can always be decomposed as

$$A = \sum_{i=1}^{\ell} r_i \text{Tr}[AO_i]\rho_i, \quad (2)$$

for a given set of coefficients r_i , observables O_i , and single-qubit states ρ_i , then the following lemma holds.

Lemma 3.1. *Let $(G(E, V), \mathcal{A})$ be a tensor network of a quantum circuit, and let $(u \rightarrow v) \in E$ be an edge in G (with $u, v \in V$). Replacing the edge $(u \rightarrow v)$ with the summation of measure-and-prepare channels as*

$$\begin{array}{ccc} u & \xrightarrow{v} & v \end{array} \equiv \sum_{i=1}^{\ell} r_i \begin{array}{c} u \\ \bullet \\ \square \\ O_i \\ \rho_i \\ v \end{array} \quad (3)$$

keeps the value of the tensor network unchanged, provided that r_i , O_i , and ρ_i satisfy (2). More precisely, by cutting the edge $(u \rightarrow v)$ and attaching a pair of \triangleleft and \triangleright vertices to the cut endpoints, the graph G is transformed into G' , and each term in the summation corresponds to a distinct tensor network (G', \mathcal{A}_i) . The value of the original tensor network $T(G, \mathcal{A})$ is then identical to

$$T(G, \mathcal{A}) = \sum_{i=1}^{\ell} r_i T(G', \mathcal{A}_i). \quad (4)$$

Proof. See Section 9.1. \square

In many quantum computing applications, a quantum circuit can be separated into disconnected subcircuits by cutting only a few wires. This allows for the simulation of large quantum circuits with more qubits than available quantum hardware can handle by executing subcircuits with different O_i and ρ_i , and reconstructing the original circuit's result using (4) [14].

The mathematical identity

$$A = \frac{\text{Tr}(AI)I + \text{Tr}(AX)X + \text{Tr}(AY)Y + \text{Tr}(AZ)Z}{2} \quad (5)$$

for any arbitrary 2×2 matrix A straightforwardly suggests an $\ell = 8$ wire cutting scheme, as suggested in [14], with

$$r_1 = +1/2, \quad O_1 = I, \quad \rho_1 = |0\rangle\langle 0|, \quad (6a)$$

$$r_2 = +1/2, \quad O_2 = I, \quad \rho_2 = |1\rangle\langle 1|, \quad (6b)$$

$$r_3 = +1/2, \quad O_3 = X, \quad \rho_3 = |+\rangle\langle +|, \quad (6c)$$

$$r_4 = -1/2, \quad O_4 = X, \quad \rho_4 = |-\rangle\langle -|, \quad (6d)$$

$$r_5 = +1/2, \quad O_5 = Y, \quad \rho_5 = |+i\rangle\langle +i|, \quad (6e)$$

$$r_6 = -1/2, \quad O_6 = Y, \quad \rho_6 = |-i\rangle\langle -i|, \quad (6f)$$

$$r_7 = +1/2, \quad O_7 = Z, \quad \rho_7 = |0\rangle\langle 0|, \quad (6g)$$

$$r_8 = -1/2, \quad O_8 = Z, \quad \rho_8 = |1\rangle\langle 1|, \quad (6h)$$

where $|\pm\rangle := (|0\rangle \pm |1\rangle)/\sqrt{2}$ and $|\pm i\rangle := (|0\rangle \pm i|1\rangle)/\sqrt{2}$ are eigenstates of X and Y , respectively. This scheme involves iterating over three different measurement bases (X , Y , and Z) and six preparation states ($|0\rangle$, $|1\rangle$, $|+\rangle$, $|-\rangle$, $|+i\rangle$, and $|-i\rangle$).

There are infinitely many possible constructions of $\{r_i\}$, $\{O_i\}$, and $\{\rho_i\}$. However, since the space of arbitrary 2×2 matrices is four-dimensional (over the complex numbers), the decomposition in (2) requires at least four preparation states. One such example is the $\ell = 4$ scheme, given by

$$\{r_i\} = \{1/2, 1/2, 1/2, 1/2\}, \quad (7a)$$

$$\{O_i\} = \{2|0\rangle\langle 0| - X, 2|1\rangle\langle 1| - Y, X, Y\}, \quad (7b)$$

$$\{\rho_i\} = \{|0\rangle\langle 0|, |1\rangle\langle 1|, |+\rangle\langle +|, |+i\rangle\langle +i|\}, \quad (7c)$$

which involves three measurement bases (X , Y , and Z) and four preparation states ($|0\rangle$, $|1\rangle$, $|+\rangle$, and $|+i\rangle$), matching the minimum number of states required. This decomposition was proposed in [19] and will be used in this section as an illustrative example.

By restricting ourselves to Pauli bases and states, which are easier to prepare and measure, we propose a generic parameterized decomposition in Section 5.2, of which the schemes in both (6) and (7) can be viewed as special cases.

The observable O_i corresponds to measuring the expectation value of O_i under specific tensor constraints. For example, the observable $|0\rangle\langle 0|$ corresponds to the probability of obtaining the $|0\rangle$ outcome, conditioned on the state of other qubits, when the qubit is measured in the Z basis. Similarly, each state ρ_i corresponds to preparing the qubit in the respective quantum state. The construction of $\{c_i\}$, $\{O_i\}$, and $\{\rho_i\}$ collectively resemble multiple measure-and-prepare channels, which form the core mechanism behind circuit cutting.

3.2 Workflow

We now shift our perspective from a theoretical view to a practical one by describing the procedure for circuit cutting. We must determine the measurement set S_{meas} and the preparation set S_{prep} , which specify the measurement bases and preparation states used at each measure-and-prepare channel. These sets can be inferred from a particular choice made for (2). For instance, given the observable set $\{O_i\}$ and the state set $\{\rho_d\}$ in (7), the measurement set

$$S_{\text{meas}} = \{X, Y, Z\} \quad (8)$$

and the preparation set

$$S_{\text{prep}} = \{|0\rangle, |1\rangle, |+\rangle, |+i\rangle\} \quad (9)$$

are sufficient, since the measurements in the X , Y , Z bases provide the results for the observables $|0\rangle\langle 0|$, $|\pm\rangle\langle \pm|$, and $|\pm i\rangle\langle \pm i|$, respectively.

After specifying the sets, the workflow for circuit cutting can generally be divided into three steps:

1. **Finding cuts.** Choose the desired cut points that divide the original circuit into multiple subcircuits. These cut points are optimally selected to minimize metrics such as postprocessing cost and sampling overhead, subject to width or depth constraints. Once

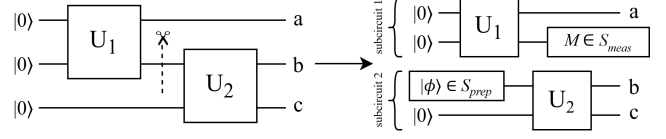


Figure 1. A 3-qubit circuit is cut into two 2-qubit subcircuits.

the subcircuits are defined, generate the *subcircuit configurations*, i.e., all possible variants of the subcircuits applying different measurement bases from S_{meas} and preparation states from S_{prep} .

2. **Executing subcircuits.** Evaluate the subcircuit configurations using classical simulation or quantum hardware. When using quantum hardware, the number of shots (as described in Section 2) must be predetermined based on the desired accuracy and selected strategies. Note that the number of subcircuit configurations scales exponentially with the number of cuts, and thus the runtime for evaluating all subcircuits will also scale exponentially unless parallel computing is applied.
3. **Postprocessing.** Combine the probability distributions obtained from the previous step according to the circuit structure and the cut parameters. Depending on what the outcome of interest is (e.g., the user may be interested in the full spectrum of all outcomes or the probability of a particular outcome), different postprocessing strategies can be applied. For an $\ell = 4$ decomposition, a total of 4^K Kronecker products are required for classical postprocessing, where K is the number of cuts [19].

3.3 Example

We now demonstrate these steps using the example shown in Figure 1, where a 3-qubit circuit is cut into two 2-qubit quantum subcircuits. We employ the decomposition (2) with the corresponding S_{meas} in (8) and S_{prep} in (9).

First, since the cut has already been located, no additional search for cut points is required. The original wire being cut gives rise to a measurement operation in subcircuit 1 and an initial state preparation in subcircuit 2. Once the subcircuits are defined by the cut, the subcircuit configurations are generated by applying different elements from S_{meas} and S_{prep} . In this case, three subcircuit configurations are generated for subcircuit 1, and four subcircuit configurations are generated for subcircuit 2.

Second, all subcircuit configurations must be evaluated. Suppose that each subcircuit configuration is evaluated on a quantum computer with 1000 shots, leading to a total of 7000 shots across the seven subcircuit configurations. If multiple quantum computers are available, these configurations can

be executed in parallel without the need for classical communication, as they are independent of one another. The output probabilities for each subcircuit configuration are computed as the ratio of the number of occurrences of each outcome to the 1000 shots.

Finally, the output probability of the original circuit can be recovered using Lemma 3.1. Let $(a, b, c) \in \{0, 1\}^3$ represent a bitstring outcome of the original circuit. Based on the decomposition in (7), the probability $p(a, b, c)$ of obtaining the bitstring outcome (a, b, c) is given by

$$p(a, b, c) = \sum_{i=1}^4 r_i p_i^{(1)}(a) p_i^{(2)}(b, c), \quad (10)$$

where r_i are given by (7a), and $p_i^{(1)}$ and $p_i^{(2)}$, defined below, are derived from the probabilities associated with the subcircuit configurations of subcircuit 1 and subcircuit 2, respectively.

In accordance with (7b), we define

$$p_1^{(1)} = 2p^{(1)}(a0|Z) - [p^{(1)}(a0|X) - p^{(1)}(a1|X)], \quad (11a)$$

$$p_2^{(1)} = 2p^{(1)}(a1|Z) - [p^{(1)}(a0|Y) - p^{(1)}(a1|Y)], \quad (11b)$$

$$p_3^{(1)} = p^{(1)}(a0|X) - p^{(1)}(a1|X), \quad (11c)$$

$$p_4^{(1)} = p^{(1)}(a0|Y) - p^{(1)}(a1|Y), \quad (11d)$$

where $p^{(1)}(a0|Z)$ represents the probability of obtaining the outcome $(a, 0)$ when measuring in the Z basis at the cut location in subcircuit 1, with similar notation applying to the other terms.

In accordance with (7c), we define

$$p_1^{(2)} = p^{(2)}(bc||0\rangle), \quad p_2^{(2)} = p^{(2)}(bc||1\rangle), \quad (12a)$$

$$p_3^{(2)} = p^{(2)}(bc||+\rangle), \quad p_4^{(2)} = p^{(2)}(bc||-i\rangle), \quad (12b)$$

where $p^{(2)}(bc||0\rangle)$ represents the probability of obtaining the outcome (b, c) when preparing the initial state $|0\rangle$ at the cut location in subcircuit 2, with similar notation applying to the other terms.

By iterating over all 8 possible bitstrings (a, b, c) , we obtain the full probability distribution of the original circuit. If only certain outcomes are of interest, we can restrict the query to those specific bitstrings. The more shots executed for each subcircuit configuration in the second step, the lower the expected error in the reconstructed probabilities. Consequently, the calculated probability of obtaining (a, b, c) will converge to the ground-truth value, provided that a sufficient number of shots are performed for each subcircuit configuration.

3.4 Sampling Overhead

In addition to the classical postprocessing cost, the sampling overhead is a major concern in the circuit-cutting scenario. The sampling overhead refers to the multiplicative factor that indicates how much the total number of shots must

be increased to achieve the same accuracy for the output probability as in the original, uncut circuit.

The sampling overhead scales as $O(16^K)$, where K is the number of cuts. In the work [13], this overhead was reduced to 4^K using randomized measurements within the Local Operations and Classical Communication (LOCC) framework. However, the LOCC framework introduces additional resource demands and potential errors due to the need for synchronization.

In this work, we adhere to the no-communication setting. Instead of reducing the theoretical sampling overhead of $O(16^K)$, we propose an adaptive approach that strategically allocates quantum resources, significantly reducing the sampling overhead in most practical cases.

4 Problem Formulation

Circuit cutting allows the simulation of large circuits using smaller ones. However, the exponential overhead in both classical resources (e.g., postprocessing costs) and quantum resources (e.g., the cost of performing measurements and state preparation) presents a significant challenge for large-scale applications. To address this, we propose a novel strategy that significantly reduces the sampling overhead associated with state preparation and measurement.

We aim for seamless integration with existing methods that minimize postprocessing costs by optimizing the locations of cuts. Accordingly, we assume that the circuit partition has been optimally determined in advance by cut-finding algorithms.

Our problem is formulated as follows: Given a quantum circuit and its partition into multiple subcircuits, the objective is to minimize the total sampling overhead required to reconstruct the output probability distribution of the original, uncut circuit within a desired level of accuracy. This is equivalent to minimizing the statistical error under constrained quantum resources, as increasing the number of shots consistently decreases the expected statistical error.

After performing a sufficient number of shots for all subcircuit configurations, we obtain estimated values for all subcircuit probabilities, such as $p^{(1)}(\cdot|\cdot)$ and $p^{(2)}(\cdot|\cdot)$ in (11) and (12), along with their variance-covariance relations, which characterize the statistical uncertainties in these estimates and the dependencies between them.

Through (4), exemplified by (10), we then compute the estimated probabilities $\{p_i\}$ for all 2^n possible bitstring outcomes $\{i\}$ of the original circuit's n qubits. The uncertainties are also propagated to $\{p_i\}$, described by a $2^n \times 2^n$ variance-covariance matrix Σ , in accordance with (10). Here, $\Sigma_{ij} \equiv \sigma_{p_i p_j}$ represents the covariance between p_i and p_j , and in particular, $\Sigma_{ii} \equiv \text{Var}(p_i)$ is the variance of p_i . This matrix Σ defines the shape of a high-dimensional Gaussian distribution centered at $\{p_i\}$ in the hyperspace constrained

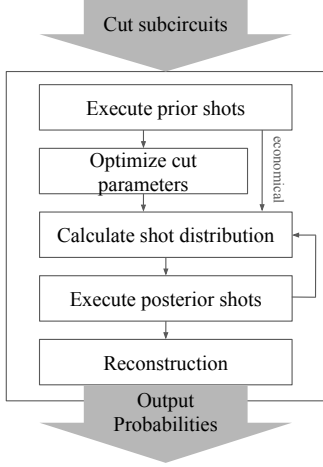


Figure 2. The workflow of ShotQC. The cut subcircuits is obtained by applying cut-finding methods on the original circuit.

by $\sum_i p_i = 1$. The Gaussian distribution represents the probability distribution for the *ground-truth* probabilities $\{\hat{p}_i\}$, given the estimates $\{p_i\}$. The eigenvalues of Σ quantify how closely $\{p_i\}$ approximates $\{\hat{p}_i\}$.²

To quantify the overall statistical uncertainty due to finite sampling, we define the *total variance* as

$$\text{Err} = \text{Tr } \Sigma \equiv \sum_{i=0}^{2^n-1} \text{Var}(p_i), \quad (13)$$

which provides a measure of the cumulative uncertainty across all probabilities $\{p_i\}$.

5 ShotQC: Framework

5.1 ShotQC: Overview

The workflow of ShotQC is depicted in Figure 2. ShotQC incorporates two novel techniques: *cut parameterization optimization* and *shot distribution optimization*. The former expands the parameter space for postprocessing without incurring additional costs, while the latter finds the optimal allocation of quantum resources to minimize the statistical error. Once the optimal cut points are identified by cut-finding algorithms, the workflow proceeds to the third block in Figure 2.

Given the disconnected subcircuits, subcircuit configurations are generated by applying different measurement bases from S_{meas} and preparation states from S_{prep} . These configurations are then executed for a predefined number of repetitions, referred to as “prior shots,” to produce a rough

²Note that one of the eigenvalues must vanish as a consequence of the constraint $\sum_i p_i = 1$. The corresponding eigenvector is the normal vector of the constrained hyperspace.

estimate P of the outcome probabilities for all subcircuit configurations.

Next, depending on the circuit size or the user’s preference, the cut parameterization optimization step is either performed—optimizing the cut parameters Θ with respect to the loss function defined in (29)—or skipped in the economical route, with Θ set to zeros.

Once Θ and P are determined, ShotQC begins the iterative process of shot distribution optimization. In each iteration, the optimal shot distribution is computed using (28), and then the subcircuit configurations are executed for a designated number of repetitions, referred to as “posterior shots,” following the optimal distribution. Based on the outcomes of these posterior shots, the estimate P is then updated.

This iterative process continues until the total number of shots reaches a predefined limit. Finally, the outcomes of all shots are aggregated, and the outcome probabilities of the original circuit are reconstructed through classical postprocessing.

5.2 ShotQC: Cut Parameterization Optimization

In Section 3.1, we establish that any decomposition of an arbitrary 2×2 matrix satisfying (2) corresponds to a valid wire-cutting scheme. This is subsequently reflected in the postprocessing phase, where the probability distribution of the original circuit is reconstructed based on the chosen decomposition, as demonstrated in Section 3.3. These findings naturally raise the question: How many valid combinations of r_i , O_i , and ρ_i are possible? Furthermore, if we extend our analysis to more general decompositions (parameterized by some “cut parameters”), can we devise a more efficient postprocessing method that further reduces statistical errors, even when utilizing the same subcircuit outcomes?

5.2.1 Problem Reduction. It turns out there are infinitely many possible choices for r_i , O_i , and ρ_i , even when O_i and ρ_i are constrained to special types, as shown below.

Mathematically, ρ_i do not necessarily need to be valid density matrices. However, in practice, ρ_i must be easy to prepare. Consequently, we restrict ρ_i to be eigenstates of the Pauli matrices X , Y , and Z . That is, we consider

$$S_{\text{prep}} = \{|0\rangle, |1\rangle, |+\rangle, |-\rangle, |+i\rangle, |-i\rangle\}, \quad (14)$$

which is the set of states used in [14]. Similarly, we impose a restriction on the observables, limiting them to the commonly available measurement set

$$S_{\text{meas}} = \{X, Y, Z\}. \quad (15)$$

With these restrictions in place, the decomposition (2) can be recast as

$$A = \sum_{i=1}^6 \sum_{j=1}^6 r_{i,j} \text{Tr}[AO_j] |\rho_i\rangle\langle\rho_i|, \quad (16)$$

where $|\rho_i\rangle \in S_{\text{prep}}$ and $O_j \in \{X_{\pm} = |\pm\rangle\langle\pm|, Y_{\pm} = |\pm i\rangle\langle\pm i|, Z_{+} = |0\rangle\langle 0|, Z_{-} = |1\rangle\langle 1|\}$, corresponding to the positive- and negative-eigenvalue outcomes of the measurement observables in S_{meas} . The decomposition then can be represented by a 6×6 table of $r_{i,j}$, where the column indexes (j) correspond to the measurement outcomes, the row indexes (i) correspond to the initial states. For instance, the decomposition (5) can be represented by Table 1. Note that we have eliminated the I observable since

$$I = I_{+} + I_{-} = |0\rangle\langle 0| + |1\rangle\langle 1| = Z_{+} + Z_{-}. \quad (17)$$

i\j	X_{+}	X_{-}	Y_{+}	Y_{-}	Z_{+}	Z_{-}
$ 0\rangle$	$1/2$	$-1/2$	0	0	0	0
$ 1\rangle$	$-1/2$	$1/2$	0	0	0	0
$ +\rangle$	0	0	$1/2$	$-1/2$	0	0
$ -\rangle$	0	0	$-1/2$	$1/2$	0	0
$ +i\rangle$	0	0	0	0	1	0
$ -i\rangle$	0	0	0	0	0	1

Table 1. The tabular representation of the decomposition described in (5).

5.2.2 Degrees of Freedom. In addition to replacing I with $Z_{+} + Z_{-}$, the decomposition allows for additional degrees of freedom, even when the set of observables and states is fixed. In particular, we observe that

$$X_{+} + X_{-} = Y_{+} + Y_{-} = Z_{+} + Z_{-} = \begin{pmatrix} 1 & 0 \\ 0 & 1 \end{pmatrix} = I, \quad (18)$$

which is an extension of (17) to all Pauli bases. By linearity, we have

$$\begin{aligned} \text{Tr}[AX_{+}] + \text{Tr}[AX_{-}] &= \text{Tr}[AY_{+}] + \text{Tr}[AY_{-}] \\ &= \text{Tr}[AZ_{+}] + \text{Tr}[AZ_{-}] \end{aligned} \quad (19)$$

for any 2×2 matrix A . This equation shows that we can adjust the coefficients $r_{i,j}$ for different O_j while preserving the validity of the decomposition, provided the equation above is satisfied. In the tabular representation, without loss of generality, for any row i , we may subtract a_i from $r_{i,1/2}$, subtract b_i from $r_{i,3/4}$, and add $a_i + b_i$ to $r_{i,5/6}$, where a_i and b_i are arbitrary real numbers.

Similarly, the same reasoning can be applied to the initial states $|\rho_i\rangle$. Since

$$\begin{aligned} |0\rangle\langle 0| + |1\rangle\langle 1| &= |+\rangle\langle +| + |-\rangle\langle -| \\ &= |+i\rangle\langle +i| + |-i\rangle\langle -i|, \end{aligned} \quad (20)$$

any adjustments to $r_{i,j}$ that preserve these relations will not compromise the validity of the decomposition. The permissible modifications in the tabular representation are analogous to those described previously, with rows and columns exchanged and a_i, b_i replaced by c_j, d_j . Incorporating all such adjustments results in Table 2, which contains a total of 24

parameters that can be arbitrarily set. We refer to this parameterized form as a “parameterized cut” and denote the set of adjustable parameters as

$$\theta = \{a_i, b_i, c_j, d_j \mid i, j = 1, \dots, 6\}, \quad (21)$$

whose significance will become evident during postprocessing. By expanding the design space for postprocessing—without the need for prior knowledge or complex constructions of initial states—we can thus explore cut parameters that minimize the statistical error during postprocessing.

5.2.3 Design Trade-offs for Overhead Reduction. While using all six states as possible options provides a total of 24 degrees of freedom, it comes at the expense of increased postprocessing cost. Instead of the original cost of 4^K Kronecker products in the $\ell = 4$ scenario, we require a total of 6^K Kronecker products for reconstruction, as $\ell = 6$. This introduces a trade-off between postprocessing cost and the number of possible states, which is directly correlated with the size of the design space. To reduce the six states to four, such as $\{|0\rangle, |1\rangle, |+\rangle, |+i\rangle\}$, certain parameters must be modified, while others are fixed. Specifically, this can be achieved by setting

$$(a_2, a_4, b_2, b_4) = (0, 0, 0, 0), \quad (22a)$$

$$(c_1, \dots, c_6) = (-1/2, 1/2, 0, 0, 0, 0), \quad (22b)$$

$$(d_1, \dots, d_6) = (0, 0, -1/2, 1/2, 0, 0), \quad (22c)$$

which reduces the degrees of freedom from 24 to 8.

Depending on the properties of the circuit cutting task, such as the number of cuts and the scale of the circuit, different design decisions can be made to balance the trade-off between the size of the design space and the classical postprocessing overhead. Since a minimum of four states is required for a valid decomposition, further reductions in the design space are not feasible. Therefore, this work primarily focuses on two options: the $\ell = 6$ case, which offers a larger design space but incurs greater classical overhead, and the $\ell = 4$ case, which has a smaller design space and lower classical overhead.

5.3 ShotQC: Shot Distribution Optimization

In the previous sections, we discussed how the output probability of the original circuit can be reconstructed using data obtained from simulating subcircuit configurations. However, not all data contribute equally in the reconstruction. For instance, consider the example shown in (10) through (12). For a given outcome bitstring $\{a, b, c\}$, if $p^{(1)}(a0|X) - p^{(1)}(a1|X) = 0$, then the outcome probability $p(a, b, c)$ is theoretically independent of $p^{(2)}(bc||+)$, as $p^{(2)}(bc||+)$ is multiplied by 0 in (10). In such cases, fewer shots are required for the configuration that generates $p^{(2)}(bc||+)$, since its statistical uncertainty will be suppressed by the estimated value of $p^{(1)}(a0|X) - p^{(1)}(a1|X)$, which is expected to be close to 0. Instead, the quantum resources can be reallocated

i\j	X_+	X_-	Y_+	Y_-	Z_+	Z_-
$ 0\rangle$	$1/2 - a_1 - c_1$	$-1/2 - a_1 - c_2$	$-b_1 - c_3$	$-b_1 - c_4$	$a_1 + b_1 - c_5$	$a_1 + b_1 - c_6$
$ 1\rangle$	$-1/2 - a_2 - c_1$	$1/2 - a_2 - c_2$	$-b_2 - c_3$	$-b_2 - c_4$	$a_2 + b_2 - c_5$	$a_2 + b_2 - c_6$
$ +\rangle$	$-a_3 - d_1$	$-a_3 - d_2$	$1/2 - b_3 - d_3$	$-1/2 - b_3 - d_4$	$a_3 + b_3 - d_5$	$a_3 + b_3 - d_6$
$ -\rangle$	$-a_4 - d_1$	$-a_4 - d_2$	$-1/2 - b_4 - d_3$	$1/2 - b_4 - d_4$	$a_4 + b_4 - d_5$	$a_4 + b_4 - d_6$
$ +i\rangle$	$-a_5 + c_1 + d_1$	$-a_5 + c_2 + d_2$	$-b_5 + c_3 + d_3$	$-b_5 + c_4 + d_4$	$1 + a_5 + b_5 + c_5 + d_5$	$a_5 + b_5 + c_6 + d_6$
$ -i\rangle$	$-a_6 + c_1 + d_1$	$-a_6 + c_2 + d_2$	$-b_6 + c_3 + d_3$	$-b_6 + c_4 + d_4$	$a_6 + b_6 + c_5 + d_5$	$1 + a_6 + b_6 + c_6 + d_6$

Table 2. The tabular representation of a generalized decomposition described in (16).

to other configurations that have a greater impact on the final result. Our main objective is to explore this concept and calculate the optimal shot distribution across all subcircuit configurations using the limited information obtained from partial sampling.

5.3.1 Calculating the Error Function. With the error function defined in (13), we investigate its relation with the number of shots across all circuit configurations.

Lemma 5.1. *Let P denote the set of estimated probabilities, and let $\Theta = \{\theta_i\}$ represent the set of all cut parameters. With a sufficient number of sampling shots N_e performed for each circuit configuration $e \in E$, the error function defined in (13) can be approximated in the form*

$$\text{Err} = \sum_{e=1}^E \frac{1}{N_e} f_e(P, \Theta), \quad (23)$$

where $f_e(P, \Theta)$ are the coefficient functions derived from the propagation of uncertainty.

Proof. See Section 9.2. \square

The coefficient function $f_e(P, \Theta)$ is computed by linearizing the reconstruction identity through differentiation and applying the propagation of uncertainty for linear combinations. In practice, if prior estimates for P are available, the error function can be approximated by substituting P with these estimates. This approach facilitates the optimization of posterior shot distribution by minimizing the error function with prior knowledge.

5.3.2 Shot Distribution. Since each configuration are simulated separately, the defined sampling overhead, or the total number of shots, is given by

$$N = \sum_{e=1}^E N_e = N_1 + N_2 + \dots + N_E. \quad (24)$$

The Cauchy-Schwarz inequality implies that

$$\left(\sum_{e=1}^E N_e \right) \left(\sum_{e=1}^E \frac{1}{N_e} f_e(P, \Theta) \right) \geq \left(\sum_{e=1}^E \sqrt{f_e(P, \Theta)} \right)^2; \quad (25)$$

in other words,

$$N \times \text{Err} \geq \left(\sum_{e=1}^E \sqrt{f_e(P, \Theta)} \right)^2. \quad (26)$$

If we treat $f_e(P, \Theta)$ as constant, which is true for a given Θ , we conclude that the error function is inversely proportional to the total number of shots. Moreover, the optimal shot distribution can be derived from this relationship, as equality holds only when the corresponding vectors are linearly dependent. Specifically, for each configuration e , we have

$$\frac{\sqrt{N_e}}{\sqrt{f_e(P, \Theta)/N_e}} = \frac{N_e}{\sqrt{f_e(P, \Theta)}} = \text{const.} \quad (27)$$

Therefore, with the total number of shots N fixed, the optimal shot distribution for each configuration e is given by

$$N_e = N \times \frac{\sqrt{f_e(P, \Theta)}}{\sum_{e=1}^E \sqrt{f_e(P, \Theta)}}. \quad (28)$$

5.3.3 Optimizing the cost function. As shown in (26), the total number of shots N required to achieve the same Err decreases if the loss function is reduced:

$$\text{Loss} = \sum_{e=1}^E \sqrt{f_e(P, \Theta)}. \quad (29)$$

Since the cut parameters Θ can be chosen arbitrarily, the loss function can be minimized by optimizing Θ . Standard optimization techniques, such as stochastic gradient descent, the Adam optimizer, or simulated annealing, can be employed.

As discussed earlier in 5.2.3, the design space for Θ can be expanded at the cost of increased classical computation. A larger design space allows for a greater range of possible parameters, enabling further reduction of the loss function's minimum value.

There are additional considerations when calculating the coefficient functions $f_e(P, \Theta)$ for determining the optimal shot allocation or minimizing the loss function. To obtain the true values of the coefficient functions, the ground-truth probabilities \hat{P} are required, or alternatively, \hat{P} must be approximated using the estimated probabilities P . Consequently, the reliability of P can affect the quality of the solutions. To address this issue, we divide the total number of shots into

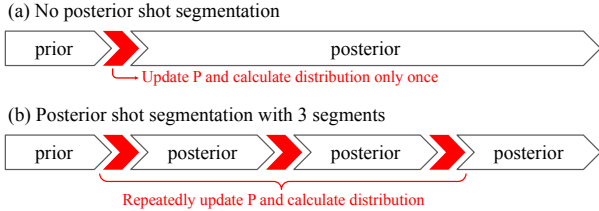


Figure 3. Posterior shot segmentation.

two stages: *prior shots* and *posterior shots*. The prior shots are performed first, with a predefined number of shots allocated to each circuit configuration to generate an initial estimate of P . This estimate is then used to calculate the optimal shot distribution for the posterior shots, which are executed in the subsequent step.

5.4 ShotQC: Additional Strategies

5.4.1 Posterior Shot Segmentation. Calculating the optimal shot distribution requires a rough estimate P of \hat{P} to begin with. Naturally, a more accurate estimate P leads to a more precise calculation of the optimal shot distribution, resulting in greater reductions in sampling overhead. However, improving the reliability of P necessitates increasing the number of prior shots. Since prior and posterior shots share the same total shot budget, allocating more shots to the prior phase reduces the number of posterior shots available for distribution. Therefore, an appropriate balance must be struck when selecting the number of prior shots to maximize overall effectiveness.

On the other hand, potential statistical bias resulting from the prior shots may cause the shot distribution to deviate from the optimal allocation. To address this issue, *posterior shot segmentation* is introduced. Instead of basing the shot distribution solely on the rough probabilities P , the posterior shots are divided into multiple stages. At each stage, the optimal shot distribution is refined using the updated estimates obtained from the previous stage. As illustrated in Figure 3, this segmentation helps mitigate the risk of prior shot bias misdirecting the overall shot distribution, ensuring a more reliable allocation process.

5.4.2 Minimal-cost Strategies. Optimizing the cut parameters Θ can often be time-consuming, due to the computationally intensive cost function that have to be calculated repeatedly with gradients for optimization. Hence, when the quantum circuit is too large, the parameters can simply be set to zeroes as described earlier. While not being able to exploit the benefits offered by cut parameterization optimization, this economical approach can still benefit from shot distribution optimization with minimum computational load. Moreover, posterior shot segmentation can also be applied with only a constant-factor increase in computational cost.

5.4.3 Output Variance Minimization. In reconstructing the output probability distribution, the variance can be further minimized by adjusting the cut parameters once again. While this approach is compatible with shot distribution optimization, we found that it often has little effect when shot distribution optimization has already been performed. This is because the final shot distribution plays a critical role in determining the variance. If the distribution is calculated for a specific set of cut parameters, altering the cut parameters disrupts this optimality, rendering variance minimization ineffective. Alternatively, when the shots are distributed equally and are independent of the cut parameters, a different strategy for adjusting the cut parameters may be applied. This approach can sometimes be more effective, particularly in cases where additional initial states are introduced. Increasing the number of initial states expands the design space, potentially enabling a lower variance minimum at the cost of greater computational overhead.

6 ShotQC: Evaluation

6.1 Evaluation Settings

To evaluate statistical error, we simulate the quantum circuits on a the aer-simulator provided by qiskit. Due to this reason, our framework is built on top of the qiskit library for integration with its classical and quantum backends. Furthermore, classical processing in ShotQC is implemented with Pytorch to enable GPU acceleration. All simulations and calculations are executed on a server with up to 10 Intel(R) Xeon(R) w7-2495X CPUs and one Nvidia RTX A4000 GPU with 16GB of memory.

We use the benchmarks in the CutQC library [19] and select the cutting points with the same toolbox. The following circuits are used:

1. *Quantum Approximate Optimization Algorithm (QAOA).* QAOA is a hybrid classical-quantum algorithm for solving combinatorial optimization problems [9]. We use QAOA circuits generated by random Erdős–Rényi graphs (denoted as erdos) and random regular graphs (denoted as regular).
2. *Supremacy.* Supremacy circuits are random circuits used to demonstrate quantum advantage by Google [3]. These circuits are highly entangled and generates dense output probabilities, making them exponentially difficult for classical computers to simulate.
3. *Adder.* Adder circuits are linear-depth ripple-carry addition circuits for arithmetic operations in quantum computing, as proposed by [8].
4. *Approximate Quantum Fourier Transform (AQFT).* AQFT is an approximate implementation of the commonly used Quantum Fourier Transform (QFT) operation that yields better performance on NISQ devices [1].

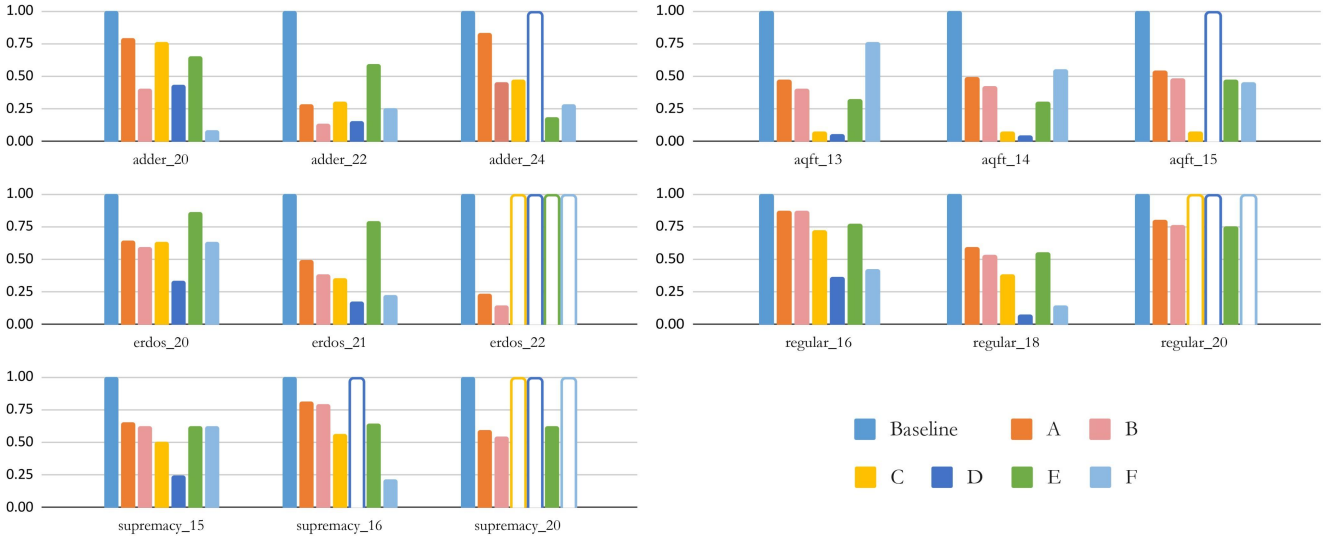


Figure 4. Simulation results: variance is normalized by the baseline. Hollow bars indicate timeout of 10 hours.

6.2 ShotQC settings

We compare the variance results of six ShotQC settings against the baseline setting with shots evenly distributed for subcircuit configurations. The six settings A–F can be categorized into three types:

- Economical Settings:** Settings A and B use minimal computational resources by avoiding optimization of the cut parameters. The prior shot ratio, defined as the fraction of prior shots to the total number of shots, is set to 0.2, and the $\ell = 4$ scheme (initial states: $|0\rangle, |1\rangle, |+\rangle, |+i\rangle$) is selected. Setting B additionally incorporates the posterior shot segmentation technique, dividing the posterior shots into 5 segments.
- Standard Settings:** Settings C and D follow the full ShotQC workflow, including the execution of prior shots, parameter optimization, and the calculation of the optimal shot distribution for posterior shots. The prior shot ratio is set to 0.2. Setting C employs the $\ell = 4$ configuration, while Setting D utilizes the $\ell = 6$ configuration (initial states: $|0\rangle, |1\rangle, |+\rangle, |-\rangle, |+i\rangle, |+i\rangle$).
- Direct-Optimize Settings:** Settings E and F implement output variance minimization as described in section 5.4.3. Setting C uses the $\ell = 4$ option, while setting D uses the $\ell = 6$ option.

6.3 Experiment Results

We compared the variance of various ShotQC methods against the baseline approach proposed in [19], with the total number of shots fixed for each circuit based on the size of the subcircuit configurations. Figure 4 illustrates the effectiveness of ShotQC across multiple circuits under different settings.

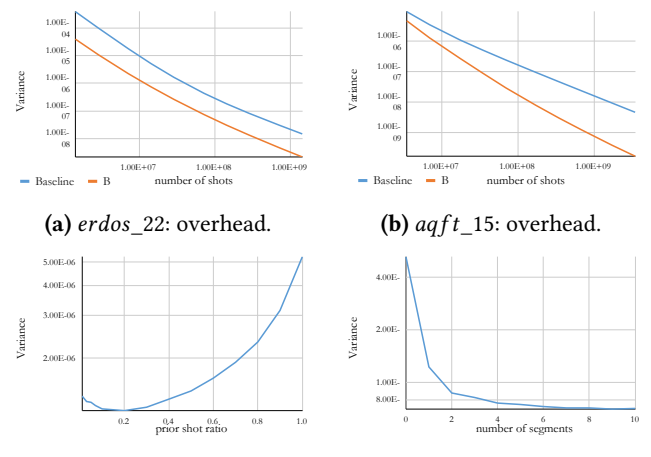


Figure 5. The effect of different parameters on variance.

On average, the best-performing settings achieve a 7.6x reduction in variance, with Setting D attaining up to a 19x reduction in the 14-qubit AQFT circuit.

Among all settings, Setting D, which incorporates both shot distribution optimization and cut parametrization, achieves the highest variance reduction in 7 out of the 15 benchmarks. However, it also encounters the most timeouts due to the computational intensity of its optimizations. In contrast, the economical Setting B achieves an average variance reduction of 2.6x without experiencing any timeouts across all 15 benchmarks, demonstrating its practicality for large-scale circuits. These results highlight a trade-off between cost and performance, suggesting that the choice of setting should depend on the specific requirements of the use case.

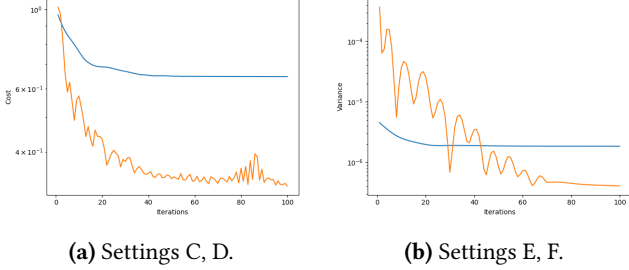


Figure 6. Optimizing cut parameters with different initial states. The blue line has $\ell = 4$, and the orange line has $\ell = 6$.

6.4 Discussions

In the experiments shown in Figure 5, ShotQC reduces variance under a fixed number of shots rather than directly reducing sampling overhead. However, as explained in Section 4, reducing variance is effectively equivalent to reducing sampling overhead. Figures 5a and 5b illustrate this relationship, comparing the baseline method to Setting B for the *erdos_22* circuit and the *aqft_15* circuit, respectively. Additionally, we observed that the effectiveness of ShotQC tends to improve as the total number of shots increases, as exemplified in Figure 5b. This improvement arises from a larger allocation of prior shots, which provides more accurate estimates for \hat{P} , enabling better calculations of the optimal shot distribution.

We also examined the impact of the prior shot ratio and the number of segments on the *erdos_22* circuit. In Figure 5c, where the number of segments is fixed at 1, an excessively high prior shot ratio reduces the number of posterior shots available for allocation, leading to increased variance. Conversely, an overly low prior shot ratio results in inaccurate estimates for output probabilities, which results in worse performance. Figure 5d shows that variance decreases rapidly at first as the number of segments increases but gradually converges. This behavior occurs because while posterior shot segmentation mitigates overshooting, it does not inherently lower variance. As a result, the benefits of posterior shot segmentation diminish quickly, as reflected in the figure.

Finally, we evaluated the optimization effectiveness under different preparation state set S_{prep} using the *adder_20* circuit with Settings C, D, E, and F. The number of optimization iterations was fixed at 100, and we compared the performance of the $\ell = 4$ and $\ell = 6$ schemes, as shown in Figure 6. Although the $\ell = 6$ scheme requires more runtime and initially performs worse than the $\ell = 4$ scheme, it eventually converges to a significantly lower loss (or variance) after more iterations. This outcome highlights the impact of introducing additional degrees of freedom, as greater flexibility enables lower minima. As in previous findings, the trade-off between classical computational cost and sampling overhead reduction must be carefully assessed for each circuit.

7 Related Works

Reducing the exponential sampling overhead is crucial for the scalability and viability for circuit cutting methods. Prior works in this field focused on finding optimal cut locations, reducing the overhead complexity by LOCC methods, and reducing the observable set.

Optimal Cut Finding Methods: Several cut finding methods have been proposed to reduce the number of cuts. CutQC utilized mixed-integer programming to locate cut locations that minimize postprocessing overhead [19], while the work of [4] considers both wire cuts and gate cuts. While gate cutting is beyond the scope of this work, ShotQC can benefit from these cut finding methods for reduction in both sampling and postprocessing overhead.

LOCC Methods: Various methods have been proposed to reduce the complexity of sampling overhead. For instance, [5] achieves a reduction from $O(16^K)$ to $O(9^K)$, while [13] further lowers it to $O(4^K)$. However, both approaches rely on LOCC settings, which restrict the parallel execution of quantum circuits and may introduce latency and fidelity challenges. In contrast, ShotQC operates independently of LOCC, making it more practical and scalable.

Observable Set Reduction: Akin to our shot distribution optimization technique, some methods leverage the imbalance of information between different observables to reduce sampling overhead. For example, RICCO [20] applies quantum state rotations at cut points to minimize the number of executions required, though this approach demands substantial optimization resources. Alternatively, methods to disregard specific basis elements have been proposed [6, 7], but they depend on either sophisticated circuit designs or favorable circumstances where the cut points naturally exhibit such properties. In contrast, ShotQC operates without requiring prior knowledge of the circuits, ensuring its applicability across a wide range of scenarios.

8 Conclusion

In this work, we present ShotQC, an enhanced circuit cutting framework for sampling overhead reduction in practical settings. ShotQC utilizes optimizations in shot distribution and cut parameterization, achieving up to a significant 19x reduction in sampling overhead during evaluation. Moreover, we proposed different ShotQC settings with trade-offs between runtime and variance reduction, allowing flexible choices for a wide variety of circuits. ShotQC motivates further research in practical overhead mitigation methods for circuit cutting, with potential further investigation into designing optimal initial states for minimum overhead.

9 Supplementary Materials

9.1 Proof of Lemma 3.1

Proof. Since every edge of the tensor network is equivalent to an identity channel, the cutting process equates to replacing an identity gate by an observable O_i on its left and a state ρ_i on its right. Thus, we have to verify that

$$\alpha A(I)\beta = \sum_{i=1}^{\ell} c_i \cdot \alpha A(O_i) \cdot A(\rho_i)\beta \quad (30)$$

to guarantee that the sum of the modified tensor networks are identical to the original. According to (1b), the left side of the equation equates to

$$\alpha A(I)\beta = \text{Tr}[M(\alpha) \cdot M(\beta)^\dagger] = \delta_{\alpha,\beta}. \quad (31)$$

Meanwhile, from (1a)(1c), the right side of the equation is

$$\begin{aligned} & \sum_{i=1}^{\ell} c_i \cdot \alpha A(O_i) \cdot A(\rho_i)\beta \\ &= \sum_{i=1}^{\ell} c_i \cdot \text{Tr}[M(\alpha)O_i] \text{Tr}[\rho_i M(\beta)^\dagger] \\ &= \sum_{i=1}^{\ell} \text{Tr}[c_i \cdot \text{Tr}[M(\alpha)O_i] \rho_i M(\beta)^\dagger] \\ &= \text{Tr}[\sum_{i=1}^{\ell} \{c_i \text{Tr}[M(\alpha)O_i] \rho_i\} M(\beta)^\dagger] \\ &= \text{Tr}[\sum_{i=1}^{\ell} \{c_i \text{Tr}[M(\alpha)O_i] \rho_i\} M(\beta)^\dagger]. \end{aligned} \quad (32)$$

Since $M(\alpha)$ is a 2×2 matrix, it satisfies $A = \sum_{i=1}^{\ell} c_i \text{Tr}[AO_i]\rho_i$ for $A = M(\alpha)$. That is,

$$\sum_{i=1}^{\ell} c_i \text{Tr}[M(\alpha)O_i]\rho_i = M(\alpha) \quad (33)$$

Therefore, the right side of equation (30) is

$$\begin{aligned} \text{Tr}[\sum_{i=1}^{\ell} \{c_i \text{Tr}[M(\alpha)O_i] \rho_i\} M(\beta)^\dagger] &= \text{Tr}[M(\alpha)M(\beta)^\dagger] \\ &= \delta_{\alpha,\beta}, \end{aligned} \quad (34)$$

which proves (30). \square

9.2 Proof of Lemma 5.1

Proof. Since the error function defined in (13) is

$$\text{Err} = \sum_{i=0}^{2^n-1} \text{Var}(p_i), \quad (35)$$

we can first consider the variance $\text{Var}(p_i)$ for some given outcome i . As demonstrated in (10) and lemma 3.1, the probability of a single outcome can be calculated by

$$p_i = \sum_{j=0}^{\ell^K-1} c_{ij} T(G', \mathcal{A}_{ij}) \quad (36)$$

with ℓ being the number of decomposition terms, K the number of cuts, and $T(G', \mathcal{A}_{ij})$ the tensor network corresponding to the cut configuration j and the outcome i .

$T(G', \mathcal{A}_{ij})$ can further be calculated by

$$T(G', \mathcal{A}_{ij}) = \prod_{x=1}^m V_{ijx}, \quad (37)$$

where V_{ijx} is the value of subcircuit x corresponding to the cut configuration j and outcome i , which is calculated by linearly combining the subcircuit probabilities such as (11)

and (12). Thus, p_i can be expressed as

$$p_i = \sum_{j=0}^{\ell^K-1} c_{ij} \left(\prod_{x=1}^m V_{ijx} \right). \quad (38)$$

When sufficient shots are taken, the variance of a function is small enough that it can be closely approximated by the variance of its first order Taylor expansion. The similar “linearization” can be applied to p_i . Collecting the terms, we have

$$\text{Var}(p_i) \approx \text{Var} \left(\sum_q g(P, \Theta, q) q \right) \quad (39)$$

with q being the probabilities used in calculating p_i and $g(P, \Theta, q)$ be its coefficient after the first order Taylor expansion. q is used as a variable when it appears in Var or Cov , and as its value otherwise. Note that since $g(P, \Theta, q)$ can be tracked during reconstruction, obtaining it takes the same time complexity for postprocessing with little to no additional cost.

Since we assume no information on the circuit, the configurations have no correlation to each other and can be treated as independent random variables. Furthermore, for each configuration e given a fixed outcome i , only a subset of its probabilities are used. These probabilities have variance

$$\text{Var}(q) = \frac{1}{N_e} q(1-q) \quad (40)$$

when the probability term q belongs to configuration e . The covariance between two probabilities q_1, q_2 in the same configuration e is

$$\text{Cov}(q_1, q_2) = -2 \cdot \frac{1}{N_e} q_1 q_2. \quad (41)$$

Thus, the variance of the can be expressed as

$$\text{Var}(p_i) = \sum_{e=1}^E \frac{1}{N_e} f_{i,e}(P, \Theta) \quad (42)$$

by expanding the variance of the linear combinations of probabilities in equation 39 with the equations provided above. By summing over all possible outcomes, we have

$$\sum_{i=0}^{2^n-1} \text{Var}(p_i) = \sum_{e=1}^E \frac{1}{N_e} f_e(P, \Theta) \quad (43)$$

where

$$f_e(P, \Theta) = \sum_{i=0}^{2^n-1} f_{i,e}(P, \Theta), \quad (44)$$

which proves the lemma.

In addition, since postprocessing takes ℓ^K terms, each term requiring inquiry to $O(6^{\#\text{meas}})$ observable probabilities for each subcircuit with $\#\text{meas}$ measure channels, leading to a complexity of $O(\ell^K \times 6^{\#\text{meas}})$. Collecting the variance and covariance terms, however, only require $\ell^{\#\text{prep}} \times 3^{\#\text{meas}}$ configurations ($\#\text{prep}$ denoting the number of prepare channels

for the subcircuit) for each subcircuit with each configuration needing $(2^{\#meas})^2 = 4^{\#meas}$ calculations, which sums up to a total complexity of $O(12^{\#meas} \times \ell^{\#prep})$. Due to the fact that for every subcircuit, we have

$$\#meas + \#prep \leq K, \quad (45)$$

the complexity for finding $f_i(P, \Theta)$ can be bounded by

$$\begin{aligned} 12^{\#meas} \times \ell^{\#prep} &\leq 12^{\#meas} \times \ell^{K-\#meas} \\ &= \ell^K \times (12/\ell)^{\#meas} \\ &\leq \ell^K \times 3^{\#meas}. \end{aligned} \quad (46)$$

The last inequality is due to the fact that $\ell \geq 4$ from Section 3.1. Hence, the complexity of obtaining the coefficient functions for all configurations $f_e(P, \Theta)$ is the same as the postprocessing process. Hence, the lemma is proven. \square

References

[1] Adriano Barenco, Artur Ekert, Kalle-Antti Suominen, and Päivi Törmä. Approximate quantum fourier transform and decoherence. *Phys. Rev. A*, 54:139–146, Jul 1996.

[2] Marvin Bechtold, Johanna Barzen, Frank Leymann, Alexander Mandl, Julian Obst, Felix Truger, and Benjamin Weder. Investigating the effect of circuit cutting in qaoa for the maxcut problem on nisq devices. *Quantum Science and Technology*, 8(4):045022, sep 2023.

[3] Sergio Boixo, Sergei V. Isakov, Vadim N. Smelyanskiy, Ryan Babbush, Nan Ding, Zhang Jiang, Michael J. Bremner, John M. Martinis, and Hartmut Neven. Characterizing quantum supremacy in near-term devices. *Nature Physics*, 14(6):595–600, Jun 2018.

[4] Sebastian Brandhofer, Ilia Polian, and Kevin Kräulich. Optimal partitioning of quantum circuits using gate cuts and wire cuts. *IEEE Transactions on Quantum Engineering*, 5:1–10, 2024.

[5] Lukas Brenner, Christophe Piveteau, and David Sutter. Optimal wire cutting with classical communication, 2023.

[6] D. T. Chen, E. H. Hansen, X. Li, V. Kulkarni, V. Chaudhary, B. Ren, Q. Guan, S. Kuppannagari, J. Liu, and S. Xu. Efficient quantum circuit cutting by neglecting basis elements. In *2023 IEEE International Parallel and Distributed Processing Symposium Workshops (IPDPSW)*, pages 517–523, Los Alamitos, CA, USA, may 2023. IEEE Computer Society.

[7] D. T. Chen, E. H. Hansen, X. Li, A. Orenstein, V. Kulkarni, V. Chaudhary, Q. Guan, J. Liu, Y. Zhang, and S. Xu. Online detection of golden circuit cutting points. In *2023 IEEE International Conference on Quantum Computing and Engineering (QCE)*, pages 26–31, Los Alamitos, CA, USA, sep 2023. IEEE Computer Society.

[8] Steven A. Cuccaro, Thomas G. Draper, Samuel A. Kutin, and David Petrie Moulton. A new quantum ripple-carry addition circuit, 2004.

[9] Edward Farhi, Jeffrey Goldstone, and Sam Gutmann. A quantum approximate optimization algorithm, 2014.

[10] Lov K. Grover. A fast quantum mechanical algorithm for database search. In *Proceedings of the Twenty-Eighth Annual ACM Symposium on Theory of Computing*, STOC ’96, page 212–219, New York, NY, USA, 1996. Association for Computing Machinery.

[11] Hiroyuki Harada, Kaito Wada, and Naoki Yamamoto. Doubly optimal parallel wire cutting without ancilla qubits, 2023.

[12] Hang Lian, Jinchen Xu, Yu Zhu, Zhiqiang Fan, Yi Liu, and Zheng Shan. Fast reconstruction algorithm based on hmc sampling. *Scientific Reports*, 13(1):17773, Oct 2023.

[13] Angus Lowe, Matija Medvidović, Anthony Hayes, Lee J. O’Riordan, Thomas R. Bromley, Juan Miguel Arrazola, and Nathan Killoran. Fast quantum circuit cutting with randomized measurements. *Quantum*, 7:934, March 2023.

[14] Tianyi Peng, Aram W. Harrow, Maris Ozols, and Xiaodi Wu. Simulating large quantum circuits on a small quantum computer. *Physical Review Letters*, 125(15), October 2020.

[15] Michael A. Perlin, Zain H. Saleem, Martin Suchara, and James C. Osborn. Quantum circuit cutting with maximum-likelihood tomography. *npj Quantum Information*, 7(1):64, Apr 2021.

[16] Alberto Peruzzo, Jarrod McClean, Peter Shadbolt, Man-Hong Yung, Xiao-Qi Zhou, Peter J. Love, Alán Aspuru-Guzik, and Jeremy L. O’Brien. A variational eigenvalue solver on a photonic quantum processor. *Nature Communications*, 5(1):4213, Jul 2014.

[17] John Preskill. Quantum Computing in the NISQ era and beyond. *Quantum*, 2:79, August 2018.

[18] P.W. Shor. Algorithms for quantum computation: discrete logarithms and factoring. In *Proceedings 35th Annual Symposium on Foundations of Computer Science*, pages 124–134, 1994.

[19] Wei Tang, Teague Tomesh, Martin Suchara, Jeffrey Larson, and Margaret Martonosi. Cutqc: using small quantum computers for large quantum circuit evaluations. In *Proceedings of the 26th ACM International Conference on Architectural Support for Programming Languages and Operating Systems*, ASPLOS ’21. ACM, April 2021.

[20] G. Uchehara, T. M. Aamodt, and O. Di Matteo. Rotation-inspired circuit cut optimization. In *2022 IEEE/ACM Third International Workshop on Quantum Computing Software (QCS)*, pages 50–56, Los Alamitos, CA, USA, nov 2022. IEEE Computer Society.

[21] Chong Ying, Bin Cheng, Youwei Zhao, He-Liang Huang, Yu-Ning Zhang, Ming Gong, Yulin Wu, Shiyu Wang, Futian Liang, Jin Lin, Yu Xu, Hui Deng, Hao Rong, Cheng-Zhi Peng, Man-Hong Yung, Xiaobo Zhu, and Jian-Wei Pan. Experimental simulation of larger quantum circuits with fewer superconducting qubits. *Phys. Rev. Lett.*, 130:110601, Mar 2023.